Bubble dynamics in a compressible liquid in contact with a rigid boundary

Wang, Qian

[Link to publication on Research at Birmingham portal](#)

Bubble dynamics in a compressible liquid in contact with a rigid boundary

Qianxi Wang [1], WenKe Liu [1], A. M. Zhang [2], Yi Sui [3]

[1] School of Mathematics, University of Birmingham, B15 2TT, United Kingdom

[2] College of Shipbuilding Engineering, Harbin Engineering University, 145, Nantong Street, Harbin

[3] School of Engineering and Materials Science, Queen Mary University of London, London E1 4NS, United Kingdom

A bubble initiated near a rigid boundary may be almost in contact with the boundary due to its expansion and migration to the boundary, where a thin layer of water forms between them thereafter. This phenomenon is modelled using the weakly compressible theory coupled with the boundary integral method. The wall effects are modelled using the method of image. The numerical instabilities caused by the near contact of the bubble surface with the boundary are handled by removing the thin layer of water between them and joining the bubble surface with its image to the boundary. Our computations correlate well with experiments for both the first- and second-cycles of oscillation. The time history of the energy of a bubble system follows a step function, reducing rapidly and significantly due to emission of shock waves at inception of a bubble and at the end of collapse but remaining approximately as a constant for the rest of the time. The bubble starts being in near contact with the boundary during the first cycle of oscillation when the dimensionless standoff distance $\gamma = s/R_m < 1$, where s is the distance of the initial bubble centre from the boundary and R_m is the maximum bubble radius. This leads to (i) the direct impact of a high speed liquid jet on the boundary once it penetrates through the bubble, (ii) the direct contact of the bubble at high temperature and high pressure with the boundary, and (iii) the direct impingement of shock waves on the boundary once emitted. These phenomena have clear potential to damage the boundary, which are believed to be the new mechanisms of cavitation damage.

Keywords: Bubble dynamics in contact with a rigid boundary; Cavitation damage; Bubble jetting; Shock waves; Local energy of a bubble system; Weakly compressible theory; Boundary integral method.

1.   Introduction

The study of bubble dynamics in the neighbourhood of a rigid boundary is associated with cavitation erosion to propellers, turbines and pumps (Plesset & Prosperetti 1977; Blake & Gibson 1987; Young 1989; Leighton 1994; Brennen 1995; Lauterborn & Kurz 2010). The cavitation damage mechanism is believed to be associated with shock waves (Rayleigh 1917; Taylor 1942) and bubble jetting (Kornfeld & Suvorov 1944; Naudé & Ellis 1961; Plesset & Chapman 1971), both are formed at the end of collapse. Similarly the damage mechanism of underwater explosion is associated with a shock wave emitted at inception of an underwater explosion bubble and bubble jetting formed at the end of collapse (Cole 1948; Klaseboer et al. 2005; Hung et al. 2010).

Recent research on ultrasound cavitation bubbles are associated with several important medical applications, including extracorporeal shock wave lithotripsy (Delius 1990; Klaseboer et al. 2007, Iloreta et al. 2008; Calvisi et al. 2008; Leighton et al. 2008, 2013), tissue ablating (histotripsy) (Roberts et al. 2006; Coussios & Roy 2007; Curtiss et al. 2013), and oncology and cardiology (Leslie & Kennedy 2006). In those applications, cavitation microbubbles absorb and concentrate significant amount of energy from ultrasound, leading to shape oscillation, violent collapsing, shock waves and bubble jetting (Wang & Manmi 2014). These mechanisms are also associated with sonochemistry (Suslick 1990; Suslick & Crum 1997) and ultrasound cavitation cleaning - one of the most effective cleaning processes for electrical and medical micro-devices (Song et al. 2004; Ohl et al. 2006).

A bubble initiated near a rigid boundary can be almost in contact with the boundary due to its expansion and migration to the boundary attracted by the second Bjerknes force (Philipp & Lauterborn 1998). This leads to the direct impact of a liquid jet on the boundary once it penetrates through the bubble, the direct contact of the bubble at minimum volume at high pressure and high temperature with the boundary, and the direct impingement of shock waves on the boundary once emitted. We believe that these phenomena have clear damage potential to the boundary. It is therefore very important to study bubble dynamics in near contact with a rigid boundary.

The boundary integral method (BIM) is grid-free in the flow domain and computationally efficient, and is thus widely used in the field of bubble dynamics. It has been applied for an axisymmetric configuration for a bubble near a rigid wall, a free surface or compliant surface (Lenoir 1979; Guerri et al. 1981; Blake et al. 1986, 1987, 1997; Zhang et al. 1993, 1994; Duncan et al. 1993, 1996; Brujan et al. 2002; Pearson et al. 2004; Wang et al. 2005; Lind & Phillips 2010, 2013; Curtiss et al. 2013) and for three dimensional configurations (Chahine et al. 1980, 1988, 1998a, b; Wang 1998, 2004; Zhang et al. 2001; Klaseboer et al. 2005, Jayaprakash et al. 2010, 2012). The BIM is suitable for an incompressible flow and does not account for the significant energy loss due to emission of shock waves associated with bubble dynamics. Lee et al. (2007) modified the BIM by removing empirically a part of the bubble potential energy at the end of the first-cycle of oscillation.

The weakly compressible theory for spherical bubbles was developed by Prosperetti & Lezzi (1986) and Lezzi & Prosperetti (1987). Wang & Blake (2010, 2011) further developed this theory for nonspherical bubbles using the method of matched asymptotic expansions. In the weakly compressible theory, the flow to second order in the outer region far away from the bubble satisfies the wave equation and is obtained analytically. The flow to second order in the inner region near the bubble satisfies Laplace's equation and thus is modelled using the BIM.

Wang (2014) modelled bubble dynamics near a rigid boundary in a compressible flow using the weakly compressible theory coupled with the BIM for the bubble initiated at $\gamma = s/R_\mathrm{m} > 1$. In this paper we will study the closer cases for $\gamma < 1$, where a part of the bubble surface starts in near contact with the rigid boundary during the expansion phase. A thin layer of water is formed between the bubble surface and the boundary and remains thin subsequently. This leads to numerical instabilities in the BIM. To avoid the numerical instabilities, we remove the thin layer of water between the bubble surface and the boundary, join the bubble surface with its image to the boundary and simulate "the combined bubble", following Ni et al. (2014). Our computations correlate well with the experiments of Philipp & Lauterborn (1998) for both the first- and second-cycles of oscillation.

2. Weakly compressible theory

Consider the dynamics of a gas bubble near a rigid flat boundary in an inviscid and compressible liquid. A Cartesian-coordinate system is set as illustrated in figure 1. The x-axis is on the rigid boundary and the z-axis is along the axis of symmetry for the configuration.
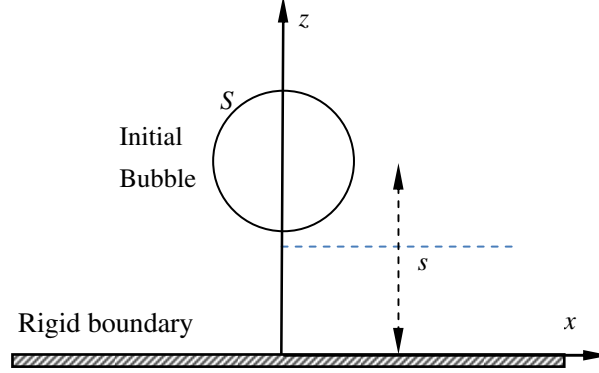

Figure 1. Illustration of a bubble near a rigid boundary, with a standoff distance s from the centre of the initial bubble to the boundary, and the coordinates used.

The maximum bubble radius R_m is chosen as the reference length, the density ρ_∞ in the undisturbed liquid is chosen as the reference density. The pressure reference is $\Delta p = p_\infty - p_v$, where p_∞ is the pressure in the undisturbed liquid and p_v is the partial pressure of vapour of the bubble. The reference velocity is thus obtained as $U = \sqrt{\Delta p / \rho_\infty}$. We perform non-dimensionalization to the problem using the reference parameters and denote dimensionless quantities by subscripts "*" as follows:

$$r_* = \frac{r}{R_m}, \qquad t_* = \frac{U}{R_m} t, \qquad \varphi_* = \frac{\varphi}{R_m U}, \qquad (2.1a, b, c)$$

$$c_* = \frac{c}{c_\infty}, \qquad p_* = \frac{p - p_\infty}{\Delta p}, \qquad (2.1d, e)$$

where $r = (x, y, z)$, t is the time, φ is the velocity potential of the liquid flow and p is the pressure. The speed of sound c is normalized by its value in the undisturbed liquid c_∞.

The compressibility of the liquid flow can be measured by the Mach number defined in terms of the reference flow velocity U and the speed of sound c_∞ in the undisturbed liquid as follows:

$$\varepsilon = \frac{U}{c_\infty}. \qquad (2.2)$$

We assume that the Mach number ε is small, because the speed of sound in water is about

4

$1500\,\mathrm{m\,s^{-1}}$, whereas the velocity of the bubble jet is lower than 200 m s^{-1} at normal ambient pressure (Benjamin & Ellis 1966; Lauterborn & Bolle 1975; Shima et al. 1981; Tomita & Shima 1986; Vogel et al. 1989, 1990; Lauterborn & Ohl 1997; Philipp & Lauterborn 1998; Lindau et al. 2003; Brujan & Matsumoto 2012; Yang et al. 2013).

We divide the fluid domain into two asymptotic regions: the inner region near the bubble where $(x, y, z) = O(R_{\mathrm{m}})$ and the outer region far away from the bubble where $(x, y, z) = O(\lambda)$, with $\lambda = c_{\infty}R_{\mathrm{m}}/U$ being the wavelength of acoustic waves. Using the method of matched asymptotic expansions, the outer solution of the velocity potential to second order has been shown to satisfy the wave equation and obtained analytically as follows (Wang 2013, 2014):

$$\varphi_*^o = -\frac{\dot{V}_*\left(t_* - \varepsilon r_*\right)}{2\pi r_*} + O\!\left(\varepsilon^2\right), \tag{2.3}$$

where the overdot denotes the derivative in time. The outer solution is due to the acoustic radiation associated with the volume oscillation of the bubble.

The inner solution of the velocity potential φ to second order satisfies Laplace's equation in the flow field and the kinematic and dynamic boundary conditions on the bubble surface S as follows:

$$\nabla_*^2\varphi_* = O\!\left(\varepsilon^2\right), \tag{2.5a}$$

$$\frac{d\boldsymbol{r}_*}{dt_*} = \nabla_*\varphi_* + O\!\left(\varepsilon^2\right) \quad \text{on } S, \tag{2.5b}$$

$$\frac{d\varphi_*}{dt_*} = 1 + \frac{1}{2}\left|\nabla_*\varphi_*\right|^2 - p_{L*} + O\!\left(\varepsilon^2\right) \quad \text{on } S. \tag{2.5c}$$

Here $p_{\mathrm{L}*}$ is the liquid pressure on the bubble surface, which is given as,

$$p_{L*} = p_{B*} - \sigma_*\nabla \cdot \mathbf{n} \quad \text{on } S, \tag{2.6a}$$

$$p_{B*} = p_{v*} + p_{g0*}\left(\frac{V_{0*}}{V_*}\right)^{\kappa}, \tag{2.6b}$$

where $p_{\mathrm{g0}*} = p_{\mathrm{g0}}/\Delta p$ is the initial partial pressure of the non-condensable gases of the bubble; V_{0*} is the initial bubble volume, and κ is the ratio of the specific heats of the gases; $\boldsymbol{n}$ is the normal vector of the bubble surface, $\nabla \cdot \mathbf{n}$ provides the surface curvature and $\sigma_* = \sigma/(R_{\mathrm{m}}\Delta p)$ is the surface tension coefficient. We assumed in (2.6b) that the pressure inside the bubble is uniform, since density of gases is usually three orders of magnitude smaller than liquids. We assume also that the expansion and contraction of the bubble gases are adiabatic. Additionally, heat and mass transfer across the bubble surface could be included (cf. Szeri et al. 2003), but

will not be considered in this paper.

The far field boundary condition of the inner solution is obtained by matching with the outer solution as follows (Wang 2014):

$$\varphi_* \to \frac{1}{2\pi}\left(\varepsilon\ddot{V}_*(t_*) - \frac{\dot{V}_*(t_*)}{r_*}\right) + O(\varepsilon^2) \quad \text{as } r_* \to \infty . \tag{2.5d}$$

The initial condition on the bubble surface is given as

$$\varphi_{n*}\big|_{t_*=0} = -R_{t*}\big|_{t_*=0} \quad \text{on } r_* = R_{0*}, \tag{2.5e}$$

where R_{0*} is the initial radius of the bubble.

Examining the initial and boundary problem of (2.5), one can see that the compressible effects appear only in the far field condition (2.5d) to the second order approximation. As the basic equation is Laplace's equation, this problem can be modeled using the BIM. The details on the numerical model using the BIM for the problem can be found in (Best 1993; Wang et al. 1996a, b).

Bubble dynamics near a flat rigid boundary are modeled using the method of image (Wang et al. 2005). When the bubble surface is nearly in contact with the rigid boundary, simulations using the BIM are often associated with numerical instabilities. To avoid the numerical instabilities, we remove the thin layer of liquid between the bubble surface and the boundary, join the bubble surface with its image to the boundary and simulate "the combined bubble" (Ni et al. 2014). In the simulations performed in this paper, the join takes place when the minimum distance δ_{min} between bubble surface and the boundary is in the range of 0.01 to 0.04.

A composite solution $\varphi_c(r_*, t_*)$ of the inner and outer solutions for the entire domain can be given as follows

$$\varphi_c(r_*, t_*) = \varphi_*(r_*, t_*) - \frac{1}{2\pi}\left(\frac{\dot{V}_*(t_* - \varepsilon r_*)}{2\pi r_*} - \frac{\dot{V}_*(t_*)}{r_*} + \varepsilon\ddot{V}_*(t_*)\right) + O(\varepsilon^2). \tag{2.6}$$

The mechanical energy of a bubble system consists of the potential energy and the kinetic energy of the bubble system. The potential energy E_P is given as follows (Wang & Manmi 2014)

$$E_{P*} = \frac{p_{g0*}V_{0*}}{\kappa-1}\left(\frac{V_{0*}}{V_*}\right)^{\kappa-1} + \sigma_* A_* + V_* , \tag{2.7}$$

where A^* is the area of the bubble surface. The reference energy is chose as $R_m^3 \Delta p$.

For a bubble system in a compressible liquid, we introduce the local kinetic energy E_{LK} of the liquid flow in the inner asymptotic region Ω_L near the bubble. Ω_L is bounded by the bubble surface S and a large sphere S_∞, with its centre at the centre of the initial bubble surface and with a radius being large compared to the bubble radius and small compared to the wavelength λ of the acoustic wave. Since the flow in the inner region satisfies Laplace's equation to second order, the local kinetic energy E_{LK} is given as follows, by using Green's divergence theorem and the outer limit of the inner solution (2.5d) (Wang 2015):

$$E_{Lk*} = \frac{1}{2}\int_{\Omega_L} \rho_* |\nabla_* \varphi_*|^2 dV = \frac{1}{2}\oint_{S+S_\infty} \varphi_* \frac{\partial \varphi_*}{\partial n} dS + O(\varepsilon^2) = \frac{1}{2}\oint_S \varphi_* \varphi_{n*} dS + O(\varepsilon).$$

(2.8)

The kinetic energy in the bubble gases are negligible since density of gases are usually three orders of magnitude smaller than liquids.

The local energy of a bubble system in a compressible liquid consists of the potential energy E_P and the local kinetic energy E_{LK} as follows:

$$E_{L*} = E_{P*} + E_{LK*} = \frac{p_{g0*}V_{0*}}{\kappa - 1}\left(\frac{V_{0*}}{V_*}\right)^{\kappa-1} + \sigma_* A_* + V_* + \frac{1}{2}\oint_S \varphi_* \varphi_{n*} dS.$$

(2.9)

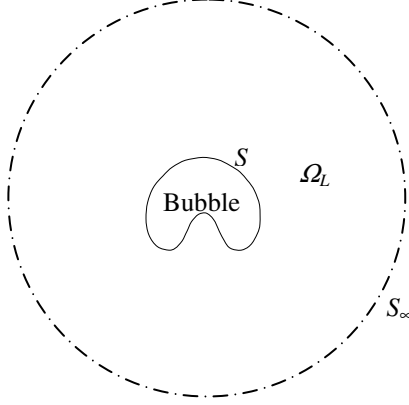

Figure 2. Illustration of the local liquid domain Ω_L bounded by the bubble surface S and a large sphere S_∞, with its centre at the centre of the initial bubble surface and with a radius R_∞.

3. Numerical analyses

The calculations are carried out for dynamics of a laser generated gas bubble at the maximum radius R_m = 1.45 mm near a rigid boundary for the dimensionless standoff distances $\gamma = s/R_m$ = 0.9, 0.6 and 0.3 respectively, to compare with the experimental data by Philipp & Lauterborn (1998). Other computational parameters are chosen as $\kappa = 1.4$, $\varepsilon = 0.013$, $\sigma_* = 0.00051$, $R_*(0)$ = 0.1, $R_{t*}(0)$ = 31 and p_{g0*} = 127 (Wang et al. 2014). The corresponding dimensional parameters are $\rho = 1000$ kgm^{-3}, $\sigma = 0.07$ Nm^{-1}, p_∞ = 98.1 kPa, p_v = 2.98 kPa, $R(0) = 1.45$ mm, $R_t(0) = 307$ ms^{-1}, $p_{g0} = 12.1$ MPa.

Figure 3 shows the bubble shapes for $\gamma = 0.9$ at typical times. The bubble expands spherically but its lower surface is flattened by the rigid boundary towards the end of expansion (figure 3a). The bubble remains almost in contact with the boundary during collapse (figure 3b), since water cannot flow from directly below into the collapsing volume. Near the end of collapse, a liquid jet forms on the distal side of the bubble surface directed towards the boundary. Once it penetrates through the bubble at t_* = 2.15 the jet impacts on the boundary immediately, which is associated with higher damage potential as compared to a jet formed away from the boundary. For the latter, the jet momentum reduces while it penetrates through the liquid before impact on the boundary.

After the jet penetrates through the bubble, a bubble ring forms. The jet pointing to the boundary is re-directed radially (away from the axis of symmetry) after it impacts on the boundary, which pushes the inner side of the bubble ring radially. As a result, the jet diameter increases causing a compression of the bubble volume from inside. In the meantime, the bubble ring collapses from other sides rapidly except for the bottom, reaching its minimum volume in near contact with the boundary at t_* = 2.30 (figures 3c), when the bubble reaches the maximum pressure and temperature (Leighton 1994; Brennen 1995; Lauterborn & Kurz 2010). This is also associated with a damage potential. In addition, a shock wave is emitted at the minimum bubble volume with high pressure amplitude (Leighton 1994; Brennen 1995; Lauterborn & Kurz 2010), it impacts on the rigid boundary once it is emitted and has another clear damage potential.

The bubble ring then rebounds mainly upwards and externally along the boundary (figure 3d). It subsequently recollapses mainly from the top and the external side (figure 3e). The radius of the bubble ring at the end of recollapse is smaller than at the end of collapse. The bubble is kept almost in contact with the boundary during the second cycle of oscillation.
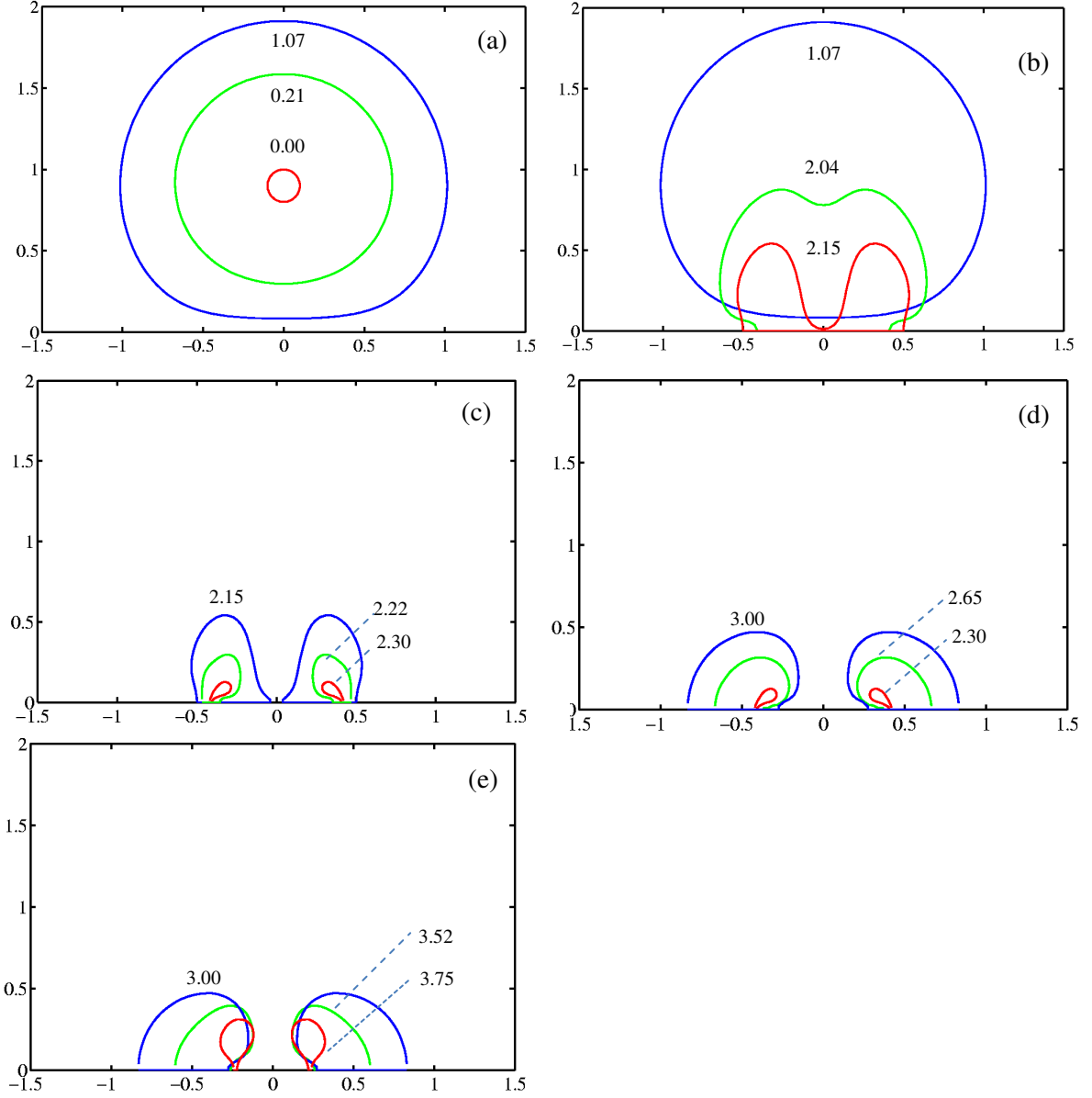
8

Figure 3. The motion of a bubble near a rigid boundary characterized by $\gamma = 0.9$, $\kappa = 1.4$, $\varepsilon = 0.013$, $\sigma_* = 0.00051$, $R_*(0) = 0.1$, $R_{t*}(0) = 31.0$ and $p_{g0*} = 127$. The bubble shapes are during (a) the 1st expansion phase, (b-c) the 1st collapse phase in a singly- and doubly-connected form respectively, (d) the 2nd expansion phase, and (e) the 2nd collapse phase.

Figures 4 and 5 show the bubble shapes at various times for $\gamma = 0.6$ and 0.3, respectively. As expected the lower part of the bubble surface starts being almost in contact with the boundary earlier than for $\gamma = 0.9$, at the middle and early stages of the expansion phase for $\gamma = 0.6$ and 0.3, as shown in figures 4a, 5a, respectively. In analogous to the case $\gamma = 0.9$, the lower part of the bubble surface keeps in near contact with the boundary subsequently and the liquid jet impacts the boundary once it penetrates through the bubble

9

(see figures 4b, 5b). Comparing figures 3b, 4b and 5b, one can see that the jet is sharper for a larger standoff distance and its width decreases with the standoff distance.

The jet is again redirected horizontally pushing away the bubble from inner side after it impacts on the boundary. The bubble ring collapses further from the all sides except for the part almost in contact with the boundary, reaching its minimum volume and maximum pressure and temperature in near contact with the boundary at $t_* = 2.32$, 2.34 respectively (figures 4c, 5c), when a shock wave is emitted and impinges on the boundary directly.

The bubble ring then further rebounds (figures 4d, 5d) and re-collapses (figures 4e, 5e), predominately from the top and external parts of the bubble surface. The radius of the bubble ring at the end of the second cycle of oscillation is again smaller than at the end of the first cycle. The maximum volume of the bubble during the second cycle increases as the bubble is initiated closer to the boundary.

We next consider the global behaviour of the bubble. Figure 6a shows the time history of the equivalent radius $R_{eq*} = \sqrt[3]{\frac{3}{4\pi} V_*}$ of the bubble for the above three cases $\gamma = 0.9$, 0.6 and 0.3, respectively. The maximum radius reduces significantly from the first to second cycles of oscillation, so does the oscillation period. The bubble maximum radius at the second-cycle are decreased to 0.56 R_m, 0.59 R_m, 0.65R_m for $\gamma = 0.9$, 0.6 and 0.3, respectively, increasing as the bubble initiated closer to the boundary.

Figure 6b shows the corresponding time history of the bubble centroid z_{cen*}. The bubble migrates slightly away from the boundary during expansion but migrates to the boundary significantly during collapse. The migration accelerates as the bubble is collapsing, reaching the maximum speed at the minimum volume. The bubble migrates the boundary faster for a larger standoff distance during the first cycle of oscillation for the three cases for $\gamma < 1.0$. This is contrary to the trend for $\gamma > 1.0$ (Wang 2014), where the bubble migrates to the boundary faster for a smaller standoff distance. This is because the nearer part of the bubble surface is retarded by the boundary during the later stage of the expansion phase as $\gamma < 1.0$ and the retarding effects start earlier for a smaller standoff distance γ.

Figure 6c shows the history of the local energy E_L of the bubble system for the cases. The local energy reduces significantly and rapidly at inception of the bubble and at the end of collapse, when shock waves are emitted. It is almost a constant during the rest of time, when the compressible effects are approximately negligible. After the shock wave is emitted at inception, about 58%, 60%, 64% of the initial energy is left for $\gamma = 0.9$, 0.6 and 0.3,

10

respectively. After the shock wave is emitted at the end of collapse, only about 14%, 22% and 23% of the initial energy is left with the bubble system for $\gamma = 0.9$, 0.6 and 0.3, respectively.

Figure 4. Bubble dynamics near a rigid boundary for $\gamma = 0.6$, with the other parameters the same as in figure 3. The bubble shapes are during (a) the 1st expansion phase, (b-c) the 1st collapse phase in a singly- and doubly-connected form respectively, (d) the 2nd expansion phase and (e) the 2nd collapse phase.
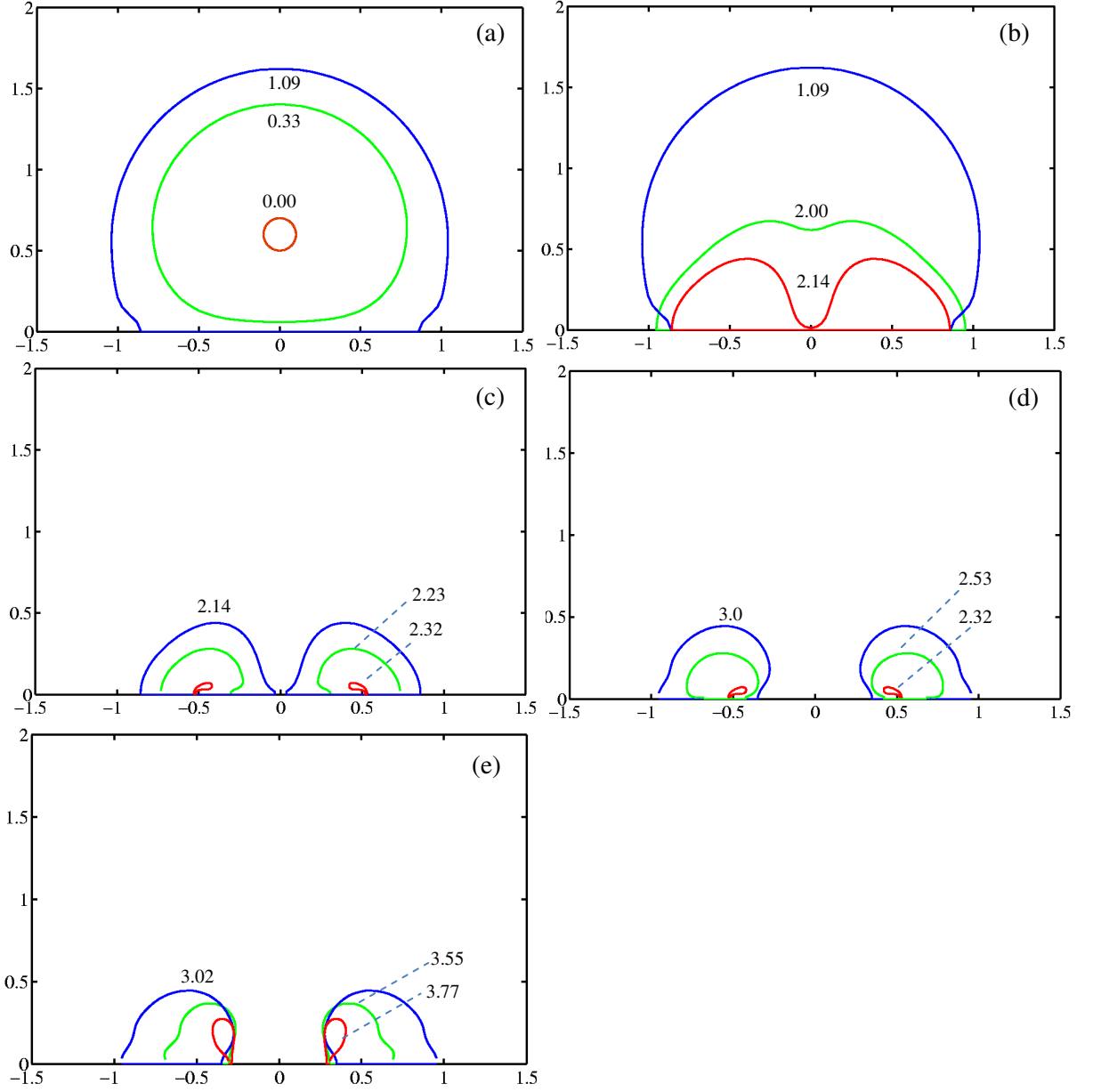
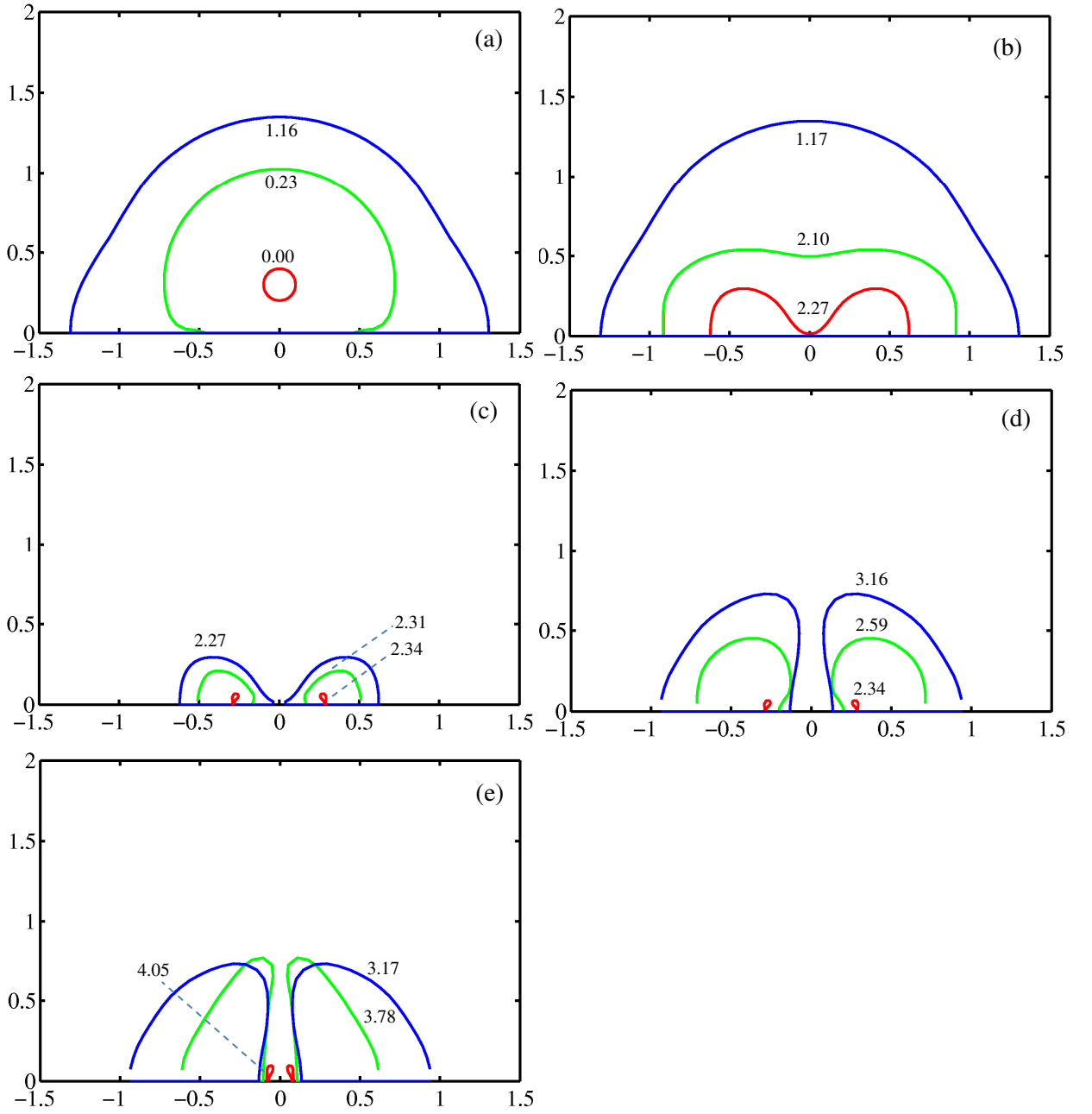Figure 5. Bubble dynamics near a rigid boundary for $\gamma = 0.3$, with the other parameters the same as in figure 3. The bubble shapes are during (a) the 1st expansion phase, (b-c) the 1st collapse phase in a singly- and doubly-connected form respectively, (d) the 2nd expansion phase and (e) the 2nd collapse phase.
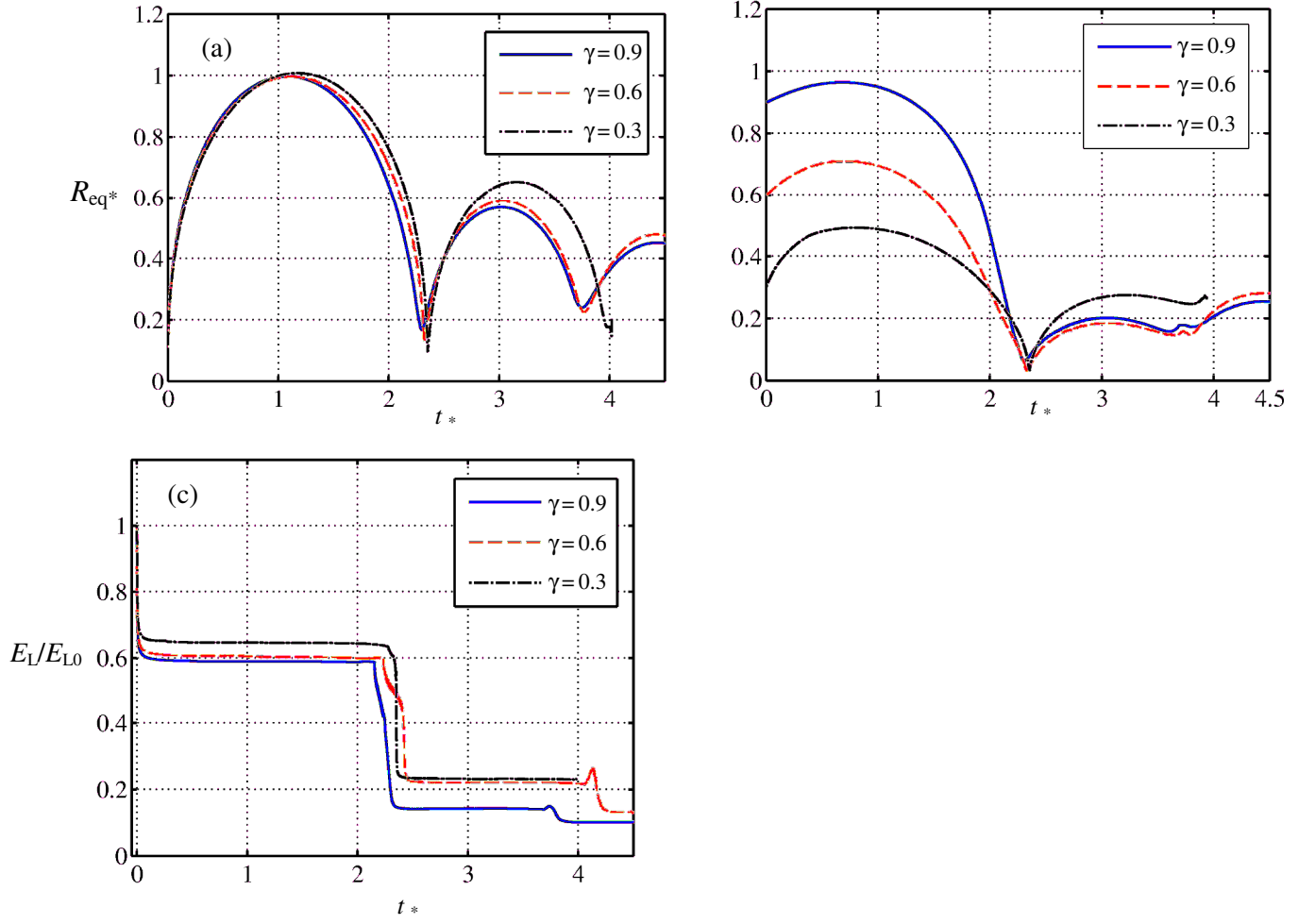
Figure 6. Time histories of (a) the equivalent bubble radius R_{eq*}, (b) z-component of the bubble centroid z_{c*}, and (c) local energy E_L/E_{L0} of the bubble system, for the cases in figures 3, 4 and 5, where E_{L0} is the initial local energy.

4. Comparison with experiments

Figure 7 shows the comparison of the bubble shapes obtained using the compressible BIM and the experiment (Philipp & Lauterborn 1998), for cavitation gas bubble dynamics near a rigid boundary for $R_m = 1.45$ mm and $\gamma = 0.9$. The experimental and computational results are shown in the left and right columns, respectively. In addition, the computational results are added overlapped with the experimental images for a direct comparison. The computation agrees very well with the experiment during the whole first cycle of oscillation (figure 7A). The expansion of the lower part of the bubble surface is retarded by the boundary at $t = 34$ μs. It approximately takes the shape of half of a sphere at its maximum volume at $t = 177$ μs, with the lower part of the bubble surface being flattened by the boundary. The upper part of the bubble surface then collapses down, assuming a cone shape at the middle stage of the collapse phase at $t = 296$ μs. The jet shown in the computational results is not visible in the experimental images due to opaqueness of the bubble surface. Nevertheless, the outer profiles of the bubble obtained in the computation and experiment agree well. The bubble ring of the computation at the end of collapse at $t = 353$ μs agrees well with the experiment, when the bubble reaches its minimum volume.

Figure 7B shows the comparison during the second cycle of oscillation. The bubble surface in the experiment is not clear due to physical instabilities occurred. Nevertheless, the bubble shapes calculated correlate with the experiment data in terms of the outer profiles at various times. Both results show that the bubble rebounds and recollapses nearly in contact with the boundary. They agree in terms of the external radius and height of the bubble ring.

A thin circular layer of water exists between the flat boundary and the lower part of the bubble surface since the later stage of the expansion phase, as the bubble is initiated with the standoff distance being less than the maximum bubble radius. It becomes an annulus thin layer after the jet penetrates the bubble. The part of the bubble surface above the thin liquid layer is almost flat and the thickness of the liquid layer does not change significantly with time. This feature is shown in the images in figure 7 from $t = 177$ to 548 μs.

It can be estimated that the vertical acceleration a_{z*} of the liquid in the thin layer is small,

$$a_{z*} = a_{z*}\big|_{z=0} + O(\varepsilon_{min}) = O(\varepsilon_{min}), \tag{4.1}$$

as $a_{z*} = 0$ on the rigid boundary. From the z-component of the Euler equation, we have

$$a_{z*} = -\partial p_* / \partial z_*. \tag{4.2}$$

The pressure in the gap can thus be estimated as follows:

14

$$p_* = p_{L*} + O(\varepsilon_{\min} a_{z*}) = p_{B*} - \sigma_* \nabla \cdot \boldsymbol{n} + O(\varepsilon_{\min}^2) = p_{B*} + O(\varepsilon_{\min}^2) = p_{B*} + O(\varepsilon_{\min}^2), \qquad (4.3)$$

where the surface tension term is neglected since the curvature radius $\nabla \cdot \mathbf{n}$ is small on the flat part of the bubble surface.

The pressure in the thin layer of liquid between the bubble and the boundary is approximately constant and equal to the pressure of the bubble gas. The flow velocity within the thin layer must be close to zero. In addition the surface tension effects intend to keep the surface flat since the pressure being constant and equal at the two sides.

A. First cycle of oscillation
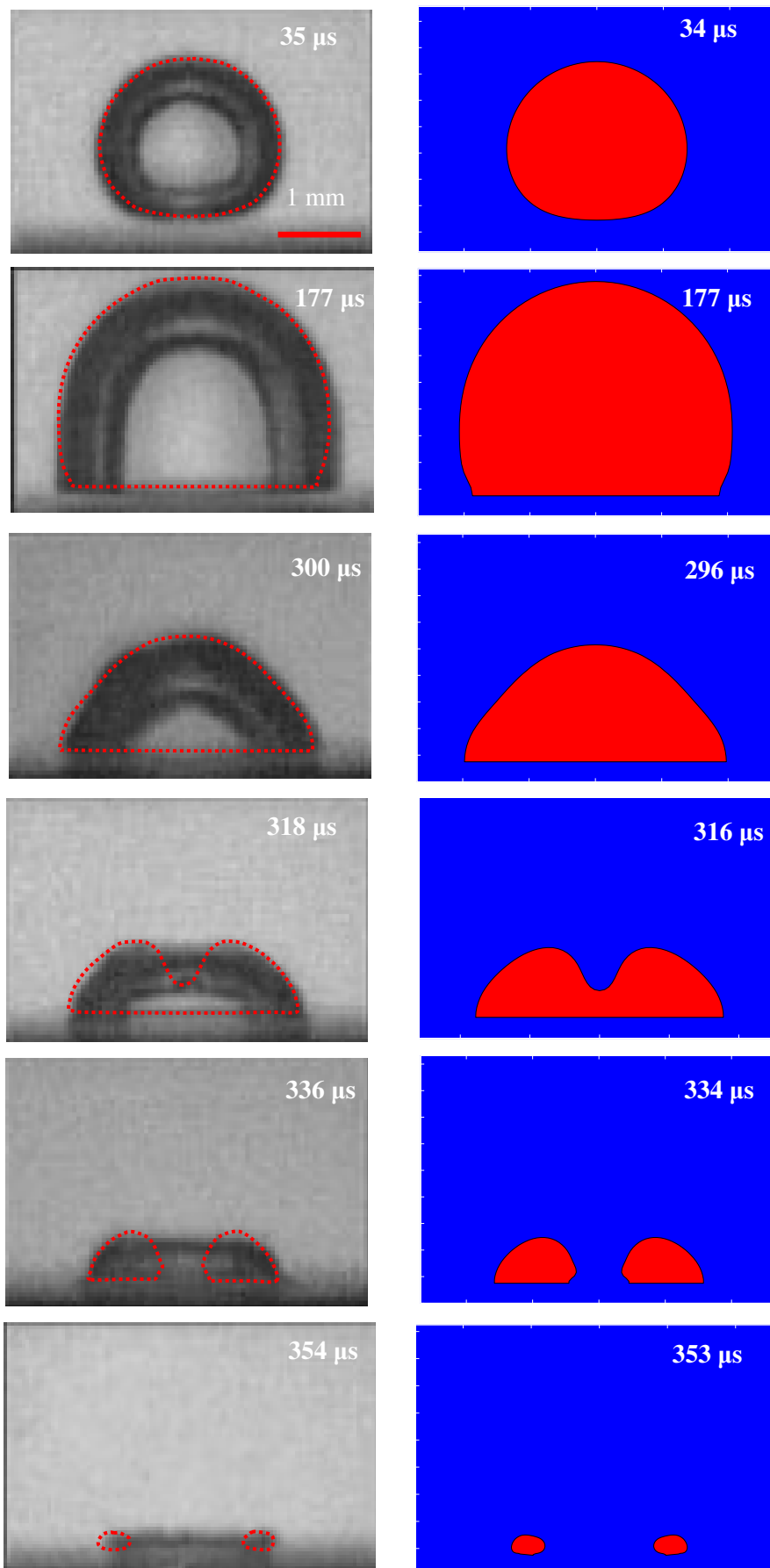
B. Second cycle of oscillation

Figure 7. Comparison of the compressible BIM computation (in the right column) with the experiment (in the left column) (reproduced with permission from Philipp & Lauterborn 1998) for the bubble shapes at various times for a cavitation bubble near a rigid boundary for $R_\mathrm{m}=$ 1.45 mm and $\gamma=0.9$: (A) during the first-cycle of oscillation and (B) during the second-cycle of oscillation. the frame width is 3.9 mm for both the computational and experimental results.

A. First collapse

Figures 8 shows the comparison between the computation and the experiment for $\gamma =$ 0.6. The computation again agrees very well with the experiment during the whole first cycle of oscillation (figure 8A). The bubble takes a shape of a half of sphere with the lower part being flattened by the wall at the middle stage of collapse at $t = 247$ μs. A bubble jet starts at $t = 285$ μs and fully develops at $t = 302$ μs. The bubble ring at the minimum volume at $t = 321$ μs calculated agrees well with the experiment. Figure 8B shows the comparison during the second cycle of oscillation. The bubble shapes calculated correlate with the experimental images. They agree well in terms of the radius and height of the bubble ring at the end of recollapse and the period of the second cycle.
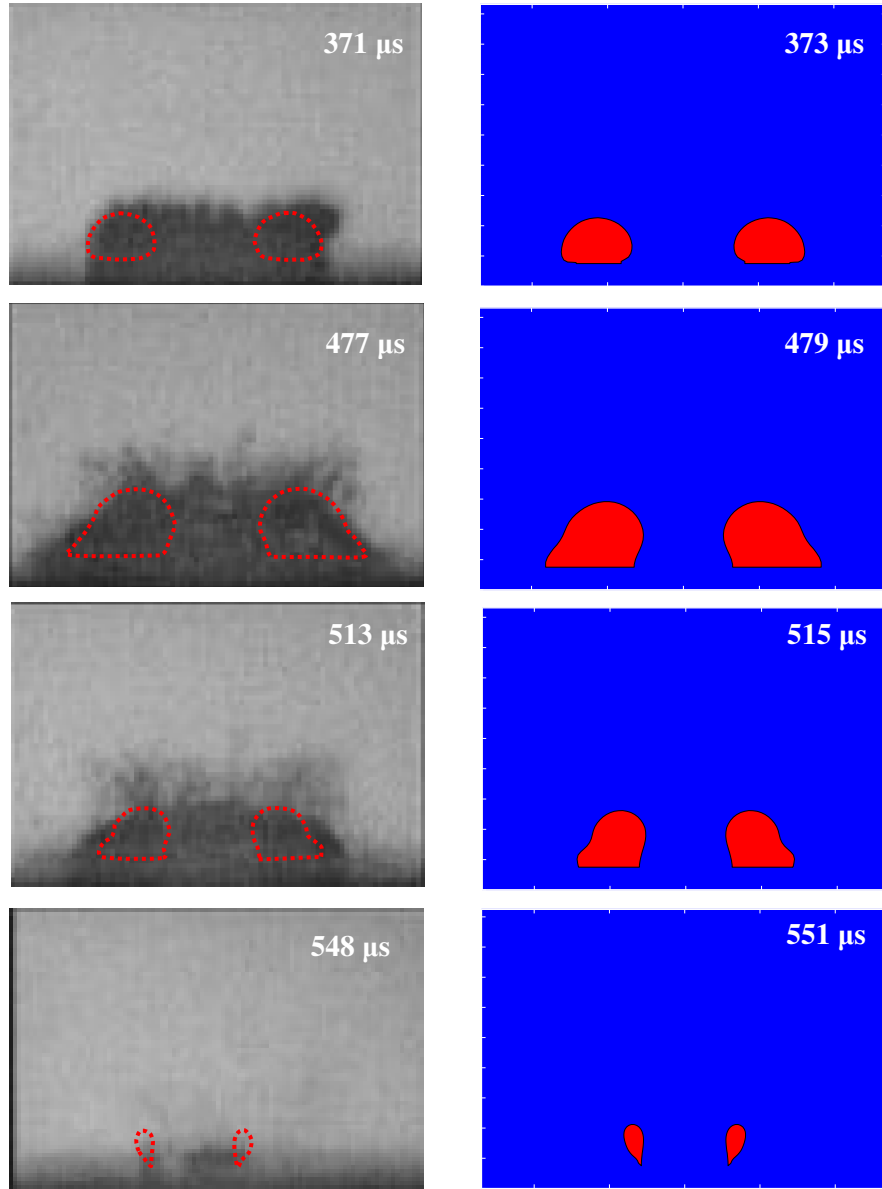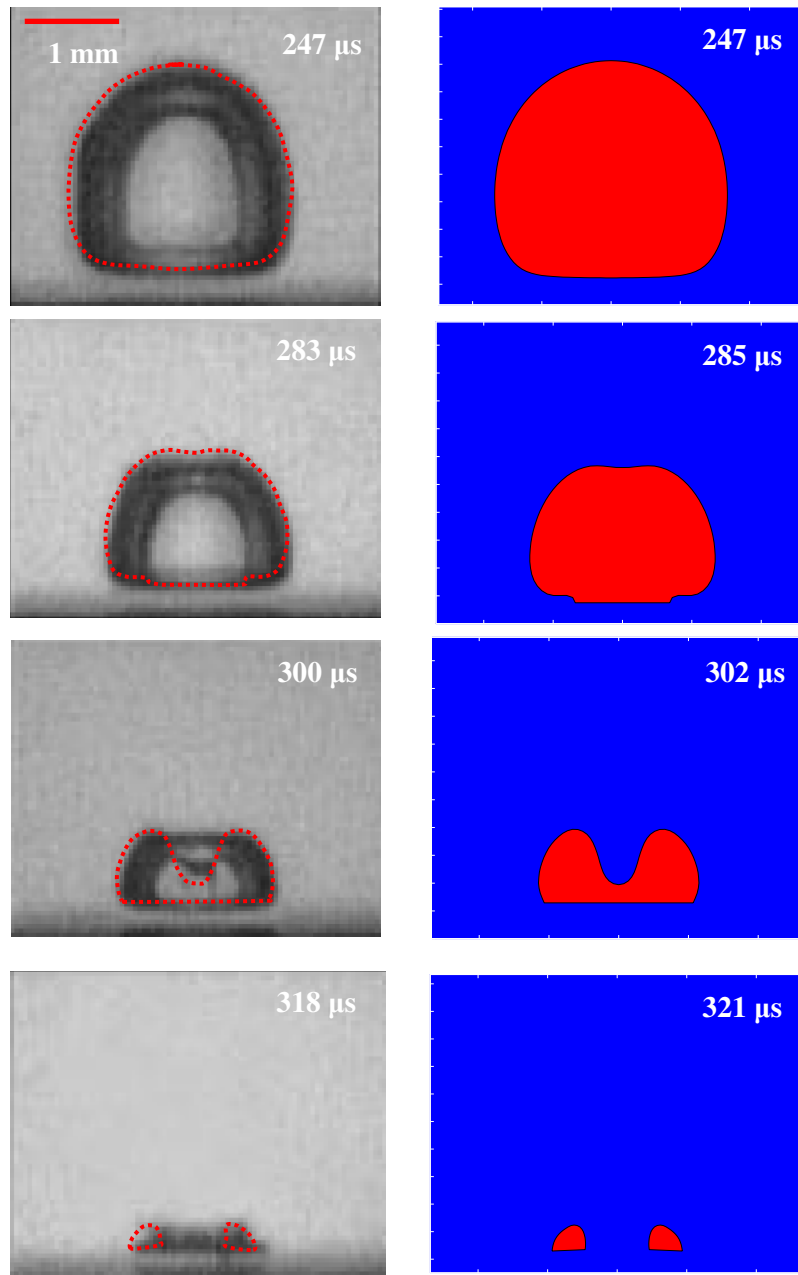
B. Second cycle of oscillation

Figure 8. Comparison of the compressible BIM computation (in the right column) with the experiment (in the left column) (Philipp & Lauterborn 1998) for the bubble shapes for $R_\mathrm{m} =$ 1.45 mm and $\gamma = 0.6$: (A) during the first-cycle of oscillation and (B) during the second-cycle of oscillation.

Figures 9 shows the comparison of the computation with the experiment for the bubble dynamics near a rigid boundary for $\gamma = 0.3$, starting from the late stage of collapse at $t = 280$ μs. The computation agrees very well with the experiment until the end of the collapse phase at $t = 354$ μs. The bubble ring calculated agrees well with the experiment during early rebounding phase to $t = 389$ μs.

A.　First collapse
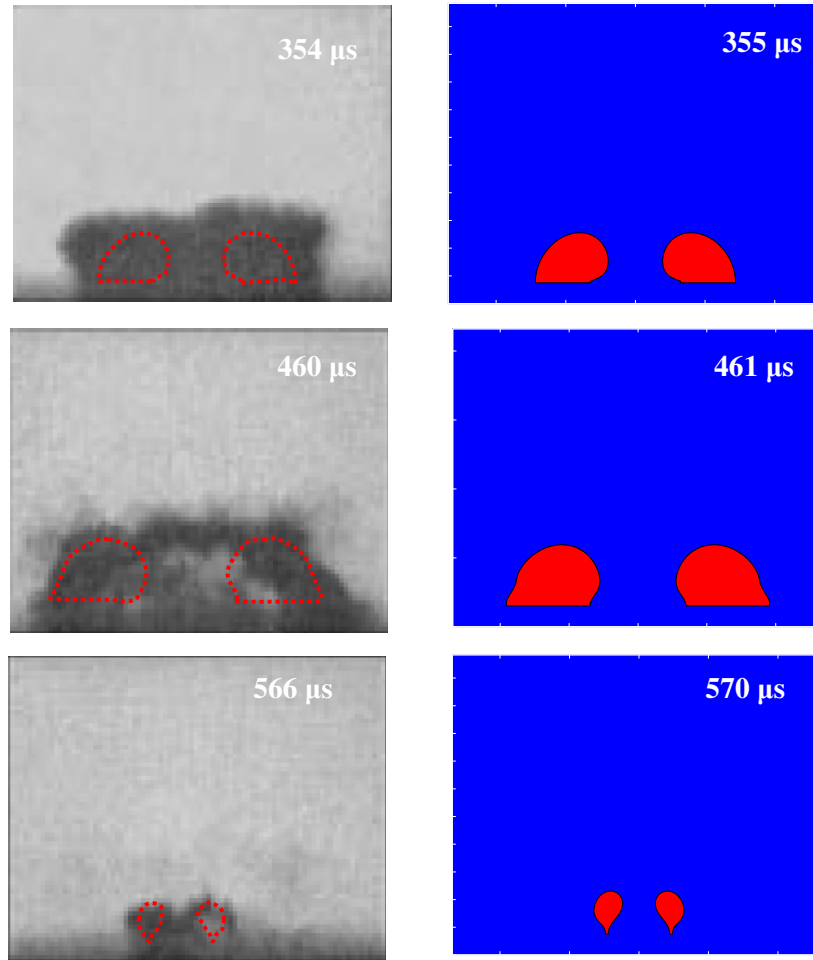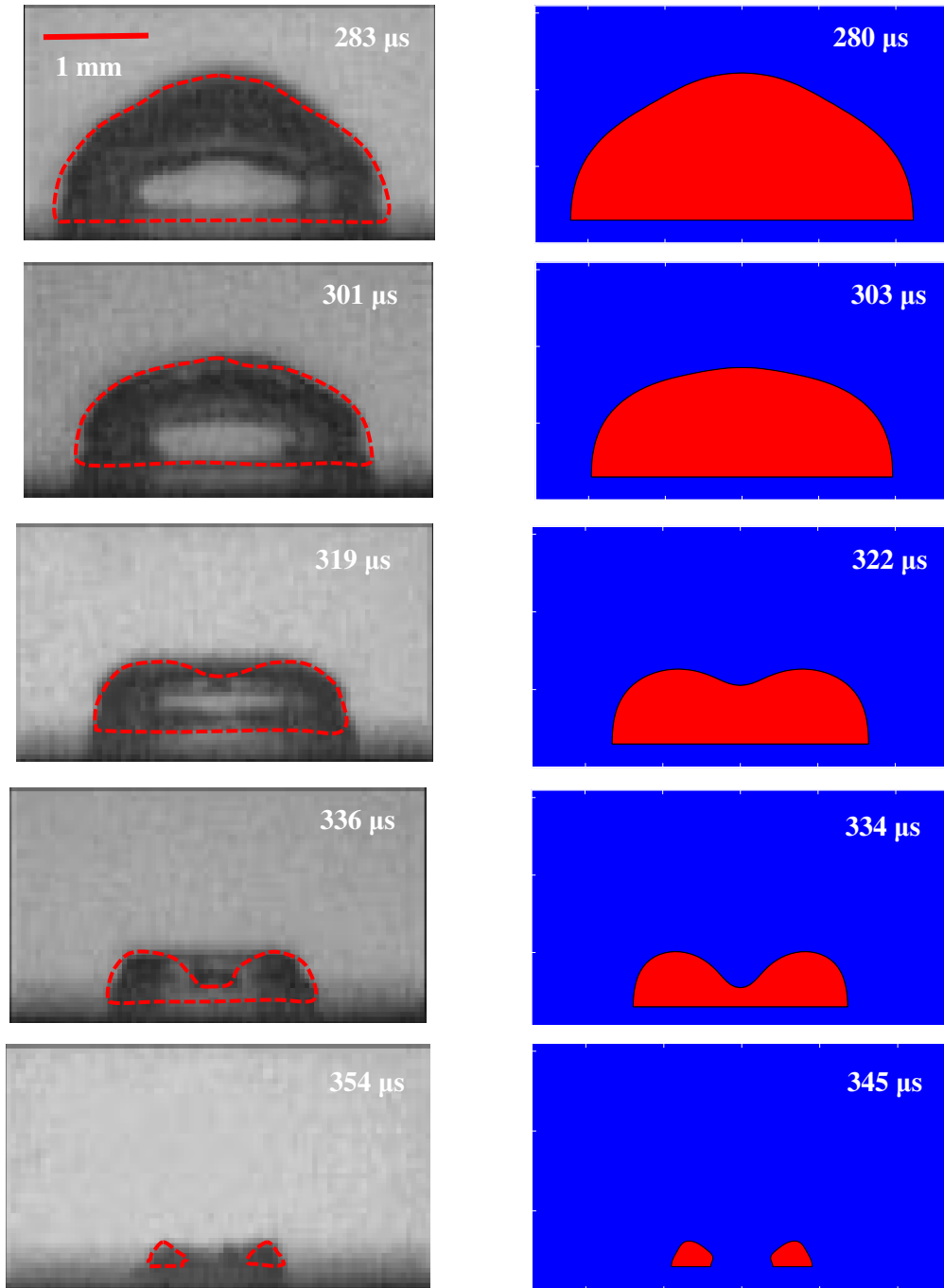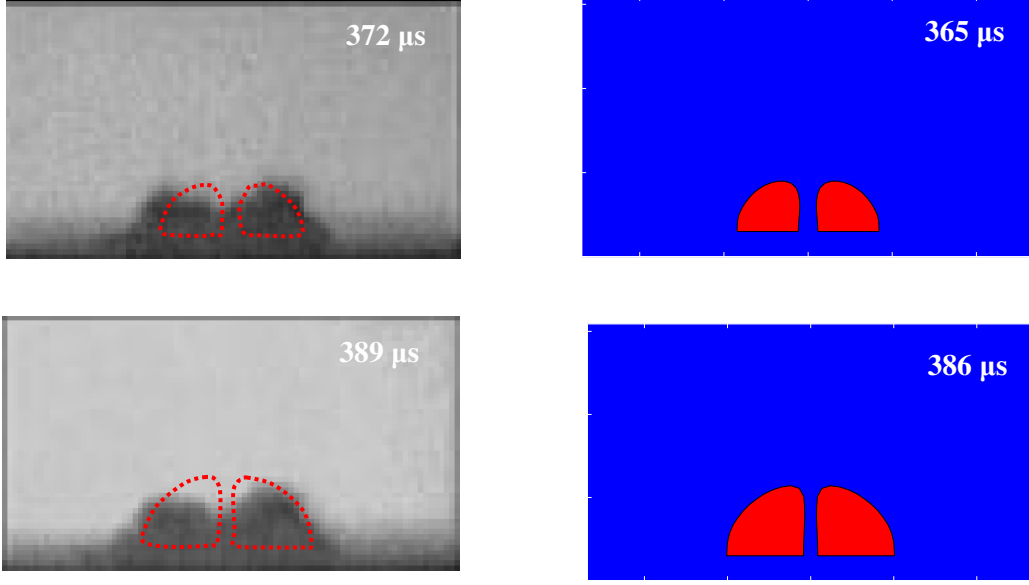
B   Second expansion

Figure 9. Comparison of the compressible BIM computation (in the right column) with the experiment (in the left column) (Philipp & Lauterborn 1998) for the bubble shapes for $R_m =$ 1.45 mm and $\gamma = 0.3$: (A) during the first-cycle of oscillation and (B) during the second-cycle of oscillation.

5.   Summary and conclusions

Bubble dynamics in nearly contact with a rigid boundary are modelled using the weakly compressible theory coupled with the boundary integral method (BIM). The near contact of the bubble surface with the boundary may cause numerical instabilities in the BIM, which is avoided by joining the bubble surface with its image to the boundary. Our computations correlate well with the experimental data for both the first- and second-cycles of oscillation.

Some of important features of the bubble dynamics near a rigid boundary have been noticed.

1.   A bubble initiated near a rigid boundary may be nearly in contact with the boundary due to its expansion and migration to the boundary, where a thin layer of water forms between them thereafter. The pressure in the thin layer of liquid is shown being approximately constant and equal to the pressure of the bubble gas. The bubble side of the thin layer remains flattened due to surface tension effects. The flow velocity within the thin layer is close to zero.

2.   The bubble starts nearly touching the rigid boundary during the expansion period when $\gamma \lesssim 1$, where γ is the dimensionless standoff distance of the bubble from the boundary in terms

21

of the equivalent maximum bubble radius. This leads to (i) the direct impact of a high speed liquid jet on the boundary once it penetrates through the bubble at the end of collapse, (ii) the direct contact of the bubble ring at high temperature and high pressure at its minimum volume with the boundary, and (iii) the direct impingement of a shock wave on the boundary once it is emitted at the end of collapse. These phenomena have clear potential to damage the boundary. We believe these three phenomena are possible new mechanisms of cavitation damage.

3. As observed in (Philipp & Lauterborn 1998; Wang 2014), the bubble starts touching the boundary during the second cycle of oscillation when $1 \lesssim \gamma \lesssim 2$. This leads to (i) the direct impact of a high speed liquid jet on the boundary once it penetrates through the bubble at the end of recollpase, (ii) the direct contact of a bubble ring at high temperature and high pressure at its second minimum volume with the boundary, and (iii) the direct impingement of a shock wave on the boundary once emitted at the end of recollapse.

4. It has been observed that the jet is sharper and thinner at a larger standoff distance.

5. The time history of the energy of the bubble system follows a step function, reducing significantly due to emissions of shock waves at its inception and the end of collapse but remaining as a constant during the rest of the time. The loss of the local energy at the end of collapse reduces with the standoff distance.

References

Benjamin, T. B. and Ellis, A. T. 1966 The collapse of cavitation bubbles and the pressure thereby produced against solid boundaries. *Phil. Trans. R. Soc. Lond.* A **260** 221–40 (doi: 10.1098/rsta.1966.0046)

Best, J. P. 1993 The formation of toroidal bubbles upon collapse of transient cavities. *J. Fluid Mech.* **251**, 79-107.(doi: 10.1017/S0022112093003349)

Blake, J. R. and Gibson, D. C. 1987 Cavitation bubbles near boundaries. *Annu. Rev. Fluid Mech.* **19**, 99-123. (doi: 10.1146/annurev.fl.19.010187.000531)

Blake, J. R., Hooton, M. C., Robinson, P. B. and Tong, P. R. 1997 Collapsing cavities, toroidal bubbles and jet impact. *Phil. Trans. R. Soc. Lond.* A **355**, 537-550. (doi: 10.1098/rsta.1997.0023)

Blake, J. R., Taib, B. B. and Doherty, G. 1986 Transient cavities near boundaries. Part 1. Rigid boundary. *J. Fluid Mech.* **170**, 479. (doi: 10.1017/S0022112086000988)

Brennen, C. E. 1995 Cavitation and Bubble Dynamics, Oxford University Press (available online). (doi: org/10.1017/CBO9781107338760)

Brujan E.A., Nahen K., Schmidt P. and Vogel A. 2001 Dynamics of laser induced cavitation bubbles near elastic boundaries: influence of the elastic modulus. J. Fluid Mech. 433, 283–314. (doi: 10.1017/S0022112000003335)

Brujan, E. A. and Matsumoto, Y. 2012 Collapse of micrometer-sized cavitation bubbles near a rigid boundary. *Microfluid Nanofluid*, **13**, 957–966. (doi: 10.1007/s10404-012-1015-6)

Calvisi, M. L., Iloreta, J. I. and Szeri, A. J. 2008 Dynamics of bubbles near a rigid surface subjected to a lithotripter shock wave: II. Reflected shock intensifies non-spherical cavitation collapse. *J. Fluid Mech.* **616** 63–97 (doi: 10.1017/S00221120080030554)

Chahine, G.L. and Bovis, A. 1980 Oscillation and collapse of a cavitation bubble in the vicinity of a two-liquid interface. Cavitation and Inhomogeneities in Underwater Acoustics, Springer-Verlag ed. New York, pp. 23-29. (doi: 10.1007/978-3-642-51070-0_3)

Chahine G.L. and Harris G. 1998a Multi-Cycle underwater explosion bubble model. Part I: Theory and validation examples for free-field bubble problems. U.S. Naval Surface Warfare Center Indian Head Division, Report IHCR 98-64, June 1998.

Chahine, G.L. and Harris, G. 1998b Multi-Cycle underwater explosion model. Part II: Validation Examples for Hull Girder Whipping Problems. U.S. Naval Surface Warfare Center Indian Head Division, Report IHCR 98-65, June 1998.

Chahine, G. L. and Perdue, T. O. 1988 Simulation of the three-dimensional behaviour of an unsteady large bubble near a structure. In Proc. 3rd Intl Colloq. on Drops and Bubbles, Monterey, CA. (doi: 10.1063/1.38981)

Cole, R. H. 1948 Underwater Explosions. Princeton University Press.

Coussios, C. C. and Roy, R. A. 2007 Applications of Acoustics and Cavitation to Non-invasive Therapy and Drug Delivery. *Annu. Rev. Fluid Mech.* **40**, 395-420. (doi: 10.1146/annurev.fluid.40.111406.102116)

Curtiss, G. A., Leppinen, D. M., Wang, Q. X. and Blake, J. R. 2013 Ultrasonic cavitation near a tissue layer. *J. Fluid Mech.* 730, 245-272. (doi: http://dx.doi.org/10.1017/jfm.2013.341)

Delius, M. 1990 Effect of lithotripter shock waves on tissues and materials. In Proc. 12th ISNA: Frontiers of Nonlinear Acoustics (ed. M. F. Hamilton and D. T. Blackstock), 31-46. Elsevier.

Duncan, J. H., Milligan, C. D. and Zhang, S. G. 1996 On the interaction between a bubble and a submerged compliant structure. *J. Sound & Vibration* **197** (1), 17-44. (doi: 10.1006/jsvi.1996.0515)

Duncan, J. H. and Zhang, S. G. 1993 On the interaction of a collapsing cavity and a compliant wall. *J. Fluid Mech.* **226**, 401-423. (doi: 10.1017/S0022112091002446)

Guerri, L., Lucca, G. and Prosperetti, A. A numerical method for the dynamics of non-spherical cavitation bubbles. Proc. 2nd Int. Colloq. on Drops and Bubbles (California, 1981), p. 175.

Hung, C. F. and Hwangfu, J. J. 2010 Experimental study of the behavior of mini-charge underwater explosion bubbles near different boundaries. J. Fluid Mech. **651**, 55-80. (doi: 10.1017/S0022112009993776)

Iloreta J. I., Fung, N. M. and Szeri A. J. 2008 Dynamics of bubbles near a rigid surface subjected to a lithotripter shock wave: I. Consequences of interference between incident and reflected waves J. Fluid Mech. **616**, 43–61(doi: http://dx.doi.org/10.1017/S0022112008003054)

Jayaprakash, A. Chao-Tsung, H. and Chahine, G. 2010 Numerical and experimental study of the interaction of a spark-generated bubble and a vertical wall. J. Fluids Engineering **134** (3), 031301-1 (doi: 10.1115/1.4005688)

Jayaprakash, A., Singh, S. and Chahine, G. 2011 Experimental and Numerical Investigation of Single Bubble Dynamics in a Two-Phase Bubbly Medium. J. Fluids Engineering **133**, 121305. (doi: 10.1115/1.4005424)

Kornfeld, M. & Suvorov, L. 1944 On the destructive action of cavitation. J. Appl. Phys. 15, 495-506. (doi: 10.1063/1.1707461)

Klaseboer, E., Fong, S. W., Turangan, C. K., Khoo, B. C., Szeri, A. J., Calvisi, M. L., Sankin, G. N. and Zhong, P. 2007 Interaction of lithotripter shockwaves with single inertial cavitation bubbles J. Fluid Mech. **593**, 33–56 (doi: 10.1017/S002211200700852X)

Klaseboer, E., Hung, K. C., Wang, C., Wang, C. W., Khoo, B. C., Boyce, P., Debono,S. and Charlier, H. 2005 Experimental and numerical investigation of the dynamics of an underwater explosion bubble near a resilient/ rigid structure. J. Fluid Mech. **537**, 387–413. (doi: 10.1017/S0022112005005306)

Lauterborn, W. and Bolle, H. 1975 Experimental investigations of cavitation-bubble collapse in the neighbourhood of a solid boundary J. Fluid Mech. **72**, 391–9. (doi: 10.1017/S0022112075003448)

Lauterborn, W. and Kurz, T. 2010 Physics of bubble oscillations. Rep. Prog. Phys. **73**,10650. (doi: 10.1088/0034-4885/73/10/106501)

Lauterborn, W. and Ohl, C. D. 1997 Cavitation bubble dynamics. Ultrasonics Sonochem. 4, 65–75. (doi: 10.1016/S1350-4177(97)00009-6)

Lauterborn, W. and Vogel, A. 2013 Shock wave emission by laser generated bubbles. In Bubble Dynamics & Shock Waves (ed. C.F. Delale), 67-103. Springer-Verlag Berlin Heidelberg. (doi: 10.1007/978-3-642-34297-4_3)

Lee, M., Klaseboer, E. and Khoo B. C. 2007 On the boundary integral method for the rebounding bubble. J. Fluid Mech. **570**, 407–429. (doi: 10.1017/S0022112006003296)

Lenoir, M. 1979 A calculation of the parameters of the high-speed jet formed in the collapse of a bubble. J. Applied Mech. Technical Phys. **20**(3), 333-337. (doi: 10.1007/BF00911690)

Lezzi, A. and Prosperetti, A. 1987 Bubble dynamics in a compressible liquid. Part. 2. Second-order theory. J. Fluid Mech. **185**, 289-321. (doi: http://dx.doi.org/10.1017/S0022112087003185)

Leslie, T. A. and Kennedy, J. E. 2006 High-intensity focused ultrasound principles, current uses, and potential for the future. Ultrasound Quart **22**, 263–272. (doi: 10.1186/2050-5736-1-9)

Leighton, T. 1994 The Acoustic Bubble. Academic Press, London. (doi: 10.1017/ S0022112094214519)

Leighton, T. G., Turangan, C.K., Jamaluddin, A.R., Ball, G.J. and White, P.R. 2013 Prediction of far-field acoustic emissions from cavitation clouds during shock wave lithotripsy for development of a clinical device. Proceedings of the Royal Society A: Mathematical, Physical and Engineering Sciences, 469, (2150), 20120538-[21pp]. (doi:10.1098/rspa.2012.0538)

Leighton, T. G., Fedele, F., Coleman, A. J., McCarthy, C., Ryves, S., Hurrell, A. M., De Stefano, A. and White, P. R. 2008 A passive acoustic device for real-time monitoring the efficacy of shockwave lithotripsy treatment. Ultrasound in Medicine & Biology, 34, (10), 1651-1665. (doi:10.1016/j.ultrasmedbio.2008.03.011)

Lind, S. J. and Phillips, T. N. 2010. The effect of viscoelasticity on a rising gas bubble. *Journal of non-Newtonian fluid mechanics* 165(15-16), pp. 852-865. (doi: 10.1016/j.jnnfm.2010.04.002)

Lind, S. J. and Phillips, T. N. 2013. The effect of viscoelasticity on the dynamics of gas bubbles near free surfaces. *Physics of Fluids* 25(2), pp. 022104-022135. (doi: 10.1063/1.4790512)

Lindau, O. and Lauterborn, W. 2003 Cinematographic observation of the collapse and rebound of a laser-produced cavitation bubble near a wall. J. Fluid Mech. **479**, 327–48 (doi: 10.1017/S0022112002003695)

Ni, B.Y., Zhang, A. M. and Wu, G.X. 2014 Numerical and experimental study of bubble impact on a solid wall. To be published in J. Eng. Flulids. (doi: 10.1115/1.4028798)

Pearson, A., Blake, J. R. and Otto, S. R. 2004 Jets in bubbles. J. Eng. Math. **48** (3-4), 391-412. (doi: 10.1023/B:engi.0000018172.53498.a2)

Philipp, A. and Lauterborn, W. 1998 Cavitation erosion by single laser-produced bubbles. J. Fluid Mech. **361**, 75–116. (doi: http://dx.doi.org/10.1017/S0022112098008738)

Plesset, M. S. and Chapman, R. B. 1971 Collapse of an initially spherical vapour cavity in the neighbourhood of a solid boundary. J. Fluid Mech. **47**, 283-290. (doi: http://dx.doi.org/10.1017/S0022112071001058)

Plesset, M. S. and Prosperetti, A. 1977 Bubble dynamics and cavitation. Ann. Rev. Fluid Mech. **9**. 145-185. (doi: 10.1146/annurev.fl.09.010177.001045)

Prosperetti, A. and Lezzi, A. 1986 Bubble dynamics in a compressible liquid. Part. 1. First-order theory. J. Fluid Mech. **168**, 457-478. (doi: 10.1017/S0022112086000460)

Ohl, C. D., Arora, M., Ikink, R., de Jong, N., Versluis, M., Delius M. & Lohse, D. 2006 Sonoporation from jetting cavitation bubbles. Biophys. J. 91, 4285-4295. (doi: org/10.1529/biophysj.105.075366)

Rayleigh, Lord 1917 On the pressure developed in a liquid during the collapse of a spherical cavity. Phil. Mag. **34**, 94–98. (doi: http://dx.doi.org/10.1017/CBO9780511704017.076)

Roberts, W. W., Hall T. L., Ives, K., Wolf, J. S., Fowlkes, J. B. and Cain, C. A. 2006 Pulsed cavitational ultrasound: a noninvasive technology for controlled tissue ablation (histotripsy) in the rabbit kidney. J. Urol. **175**, 734–738. (doi: 10.1016/S0022-5347(05)00141-2)

Shima, A., Takayama, K., Tomita, Y. and Miura, N. 1981 An experimental study on effects of a solid wall on the motion of bubbles and shock waves in bubble collapse. Acustica 48, 293-301.

Song, W.D., Hong, M.H., Luk'yanchuk, B. and Chong, T.C., 2004 Laser-induced cavitation bubbles for cleaning of solid surfaces. J. Appl. Phys. **95** (6): 2952. (doi: org/+10.1063/1.1650531)

Suslick, K. S. 1990 Sonochemistry. Science 247, 1439–1445.

Suslick, K. S. & Crum, L. A. 1997 in Encyclopedia of Acoustics (ed. Crocker, M. J.) 271-282 Wiley-Interscience, New York,).

Szeri, A. J., Storey, B. D., Pearson, A. and Blake, J. R. 2003 Heat and mass transfer during the violent collapse of nonspherical bubbles. Phys. Fluids **15**, 2576–2586. (doi: 10.1063/1.1595647)

Taylor, G. I. 1942 Vertical motion of a spherical bubble and the pressure surrounding it. In Underwater Explosion Research, **2**, 131–144, Office of Naval Research, Washington, DC.

Tomita, Y. and Shima, A. 1986 Mechanisms of impulsive pressure generation and damage pit formation by bubble collapse. J. Fluid Mech. **169**, 535–564. (doi: 10.1017/S0022112086000745)

Vogel, A., Lauterborn, W. and Timm, R. 1989 Optical and acoustic investigations of the dynamics of laser-produced cavitation bubbles near a solid boundary. J. Fluid Mech. **206**, 299–338. (doi: http://dx.doi.org/10.1017/S0022112089002314)

Vogel, A., Schweiger, P., Frieser, A., Asiyo, M. and Birngruber, R. 1990 Intraocular Nd:YAG laser surgery: damage mechanism, damage range and reduction of collateral effects. IEEE J. Quant. Electr. **26**, 2240-2260. (doi: 10.1109/3.64361)

Wang, Q. X. 1998 The numerical analyses of the evolution of a gas bubble near an inclined wall. Theoret. & Comput. Fluid Dyn. **12**, 29-51.

Wang, Q. X. 2004 Numerical modelling of violent bubble motion. Phys. Fluids **16** (5), 1610-1619. (doi: 10.1063/1.1704645)

Wang, Q. X. 2013 Underwater explosion bubble dynamics in a compressible liquid. Phys. Fluids **25**, 072104. (doi: http://dx.doi.org/10.1063/1.4812659)

Wang, Q. X. 2014 Multi-oscillations of a bubble in a compressible liquid near a rigid boundary, J. Fluid Mech. 745, 509-536. (doi: 10.1017/jfm.2014.105. 509)

Wang, Q. X. 2015 Where does the energy of a violently collapsing bubble system go? Submitted to J. Fluid Mech.

Wang, Q. X. and Blake, J. R. 2010 Non-spherical bubble dynamics in a compressible liquid. Part 1. Travelling acoustic wave. J. Fluid Mech. **659**, 191-224. (doi: 10.1017/S0022112010002430)

Wang, Q. X. and Blake J. R. 2011 Non-spherical bubble dynamics in a compressible liquid. Part 2. Acoustic standing wave. J. Fluid Mech. **679**, 559-581. (doi: 10.1017/jfm.2011.149. 559)

Wang, Q. X. & Manmi K. 2014 Microbubble dynamics near a wall subjected to a travelling acoustic wave. Phys. Fluids 26, 032104.

Wang, Q. X., Yeo, K. S., Khoo, B. C. and Lam, K. Y. 1996a Nonlinear interaction between gas bubble and free surface. Computers & Fluids **25** (7), 607. (doi: 10.1016/0045-7930(96)00007-2)

Wang, Q. X., Yeo, K. S., Khoo, B. C. and Lam, K. Y. 1996b Strong interaction between buoyancy bubble and free surface. Theor . Comput. Fluid Dyn. **8**, 73. (doi: 10.1007/BF00312403)

Wang, Q. X., Yeo, K. S., Khoo, B. C. and Lam, K. Y. 2005 Vortex ring modelling for toroidal bubbles. Theoret. & Comput. Fluid Dyn. **19** (5), 303-317. (doi: 10.1007/s00162-005-0164-6)

Yang, Y. X., Wang, Q. X. and Keat, T. S. 2013 Dynamic features of a laser-induced cavitation bubble near a solid boundary. Ultrasonics Sonochemistry 01. (doi: 10.1016/j.ultsonch.2013.01.010)

Young, F. R. 1989 Cavitation. McGraw-Hill.

Zhang, S. G. and Duncan, J. H. 1994 On the non-spherical collapse and rebound of a cavitation bubble. Phys. Fluids **6** (7), 2352–2362. (doi: 10.1063/1.868185)

Zhang, S. G, Duncan, J. H., and Chahine G. L. 1993 The final stage of the collapse of a cavitation bubble near a rigid wall. J. Fluid Mech. **257** 147-181. (doi: 10.1017/S0022112093003027)

Zhang, Y. and Li, S. C. 2014. Mass transfer during radial oscillations of gas bubbles in viscoelastic mediums under acoustic excitation. Int. J. Heat Mass Transfer, 69, 106-116. (doi: 10.1016/j.ijheatmasstransfer.2013.10.019)

Zhang, Y. L., Yeo, K. S. Khoo, B. C. and Wang, C. 2001 3D jet impact and toroidal bubbles. J. Comput. Phys. 166 (2), 336–360. (doi: 10.1006/jcph.2000.6658)